

Solar polarimetry close to the diffraction limit

Christoph U. Keller*

National Solar Observatory, 950 N. Cherry Ave., Tucson, AZ 85719

ABSTRACT

Much progress has been made during the last years in obtaining polarimetric observations of the Sun close to the diffraction limit. Here I summarize the problems one encounters when observing close to the diffraction limit of a large solar telescope, review techniques, present examples of recent observations, and discuss the need for further developments of instruments and image reconstruction techniques.

Keywords: Sun, polarimetry, adaptive optics, image reconstruction

1. INTRODUCTION

Spatial structures in the solar photosphere associated with purely hydrostatic phenomena are likely to be seen down to scales of the order of the pressure scale height and the photon mean free path, which are about 70 km (=0.1 arcsec at disk center) in the lower photosphere. Dynamic structures and magnetic fields, however, will be visible at even smaller scales. Existing solar telescopes have diameters of less than 1.5 m. Hence, even in the visible part of the spectrum, the scales of solar structures extend out to the diffraction limit of current solar telescopes. Based on numerical magneto-hydrodynamic simulations¹, future solar telescopes such as the Advanced Technology Solar Telescope (ATST)² with its 4-m aperture are expected to see magnetic structures down to their diffraction limit even at visible wavelengths.

The best diagnostic for magnetic fields on the Sun is the polarization of spectral lines. In the presence of a magnetic field, the Zeeman effect leads to a splitting of spectral lines into several components. These components are circularly polarized in the case of the magnetic field vector being parallel to the line of sight, and linearly polarized in the case of a field perpendicular to the line of sight. The splitting of spectral lines in the visible is most prominent in the large, strong fields of sunspots and pores. In the much smaller magnetic elements, whose size is close to the diffraction limit of current solar telescopes, the splitting is not easily detected in intensity profiles since these tiny features are mostly unresolved. However, the polarization signature in spectral lines is easily measured since the non-magnetic part of the solar atmosphere does not contribute to the polarization signal (with the exception of linear scattering polarization very close to the solar limb).

The achievable spatial resolution has typically been limited by the turbulence in the Earth's atmosphere (seeing). To overcome this resolution limit, various techniques have been developed to achieve diffraction-limited resolution even for polarimetric observations that require long effective exposure times. While solar adaptive optics has made rapid progress in the last few years^{3,4}, post-facto image reconstruction techniques are still required to remove the influence of aberrations that have not been fully compensated by the adaptive optics system. This is particularly important for fields of view larger than a few arcsec because even a perfect AO system can only fully correct the aberrations over a small field of view whose diameter is given by the isoplanatic angle. Since many solar features and phenomena need to be studied over larger fields of view than the isoplanatic patch would provide, adaptive optics needs to be combined with post-facto reconstruction techniques to reach the diffraction limit over the required field of view. Only solar multi-conjugate adaptive optics (MCAO) might render image-reconstruction techniques superfluous.

Section 2 summarizes the general problem of polarimetric observations close to the diffraction limit of a large solar telescope. Large in this context is defined as a telescope whose spatial resolution without an adaptive optics system is limited by seeing and not by diffraction. Sections 3 to 6 introduce some of the post-facto reconstruction techniques used

* ckeller@noao.edu; phone (520) 318-8445; <http://www.noao.edu/noao/staff/keller>

to reach the diffraction limit in magnetic field maps and illustrate this with examples of recent observations. Section 7 discusses instrumental concepts for future diffraction-limited polarimetry. I conclude with a short discussion and outlook.

2. PHOTON STARVATION CLOSE TO THE DIFFRACTION LIMIT

Even though the Sun is the brightest object in the sky, solar spectroscopic observations with spatial pixel sizes appropriate for diffraction-limited resolution are photon-noise limited. This is because the time resolution also has a major influence. The number of photons per wavelength interval, per time interval, and per angular resolution element is independent of the aperture size at the diffraction limit. Photospheric intensity patterns can move with apparent speeds of up to 7 km/s. For features 0.1 arcsec or smaller in size, one must collect photons for only a few seconds to avoid spatial smearing. Thus, the total number of available photons collected with diffraction-limited spatial resolution actually (linearly) decreases with increasing aperture. To obtain the necessary signal-to-noise ratio at a given spatial resolution, the required aperture is larger than what is required by diffraction alone. For instance, a diagnostically accurate measurement of the vector magnetic field at 0.1-arcsec resolution and 5-second maximum integration time requires a 4-m aperture, despite the fact that a 1.5-m telescope would provide adequate spatial resolution.

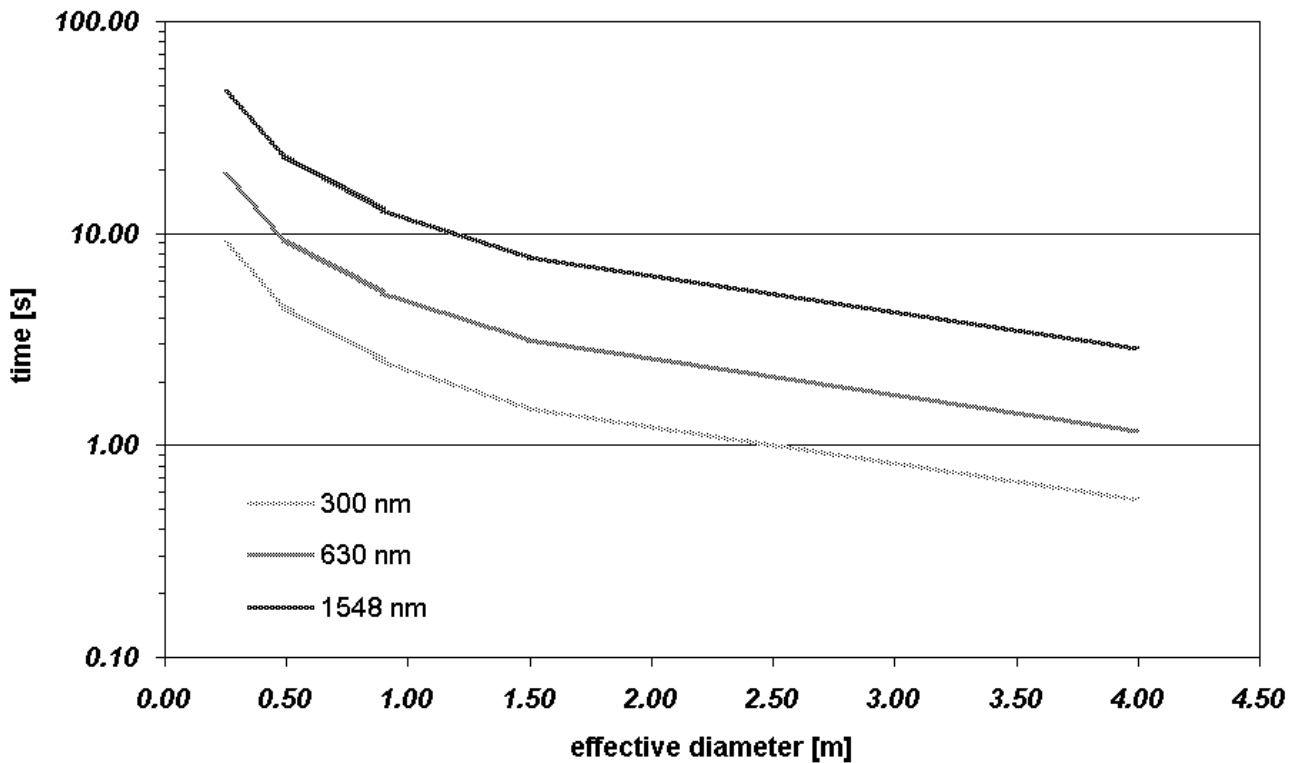


Fig. 1: Maximum possible exposure time at the diffraction limit as a function of effective aperture for a realistic solar telescope. If the exposure time is longer, smearing due to the evolution of solar features during the exposure will occur. The calculations extend from a 25-cm effective aperture diameter up to 4 m, currently the largest planned solar telescope aperture.

A few simple calculations illustrate this issue in more detail. Let us assume that we have:

- An unobscured aperture;
- 10% overall efficiency (including detectors), which is high for typical solar telescopes and instruments;
- A maximum horizontal motion of solar features of 5 km/s, which is close to the sound speed in the lower photosphere;

- An effective integration time given by the requirement that the solar image does not evolve more than half a pixel during the integration time;
- A spectral resolution of 150,000;
- Nyquist sampling in space (diffraction-limited) and spectrum.

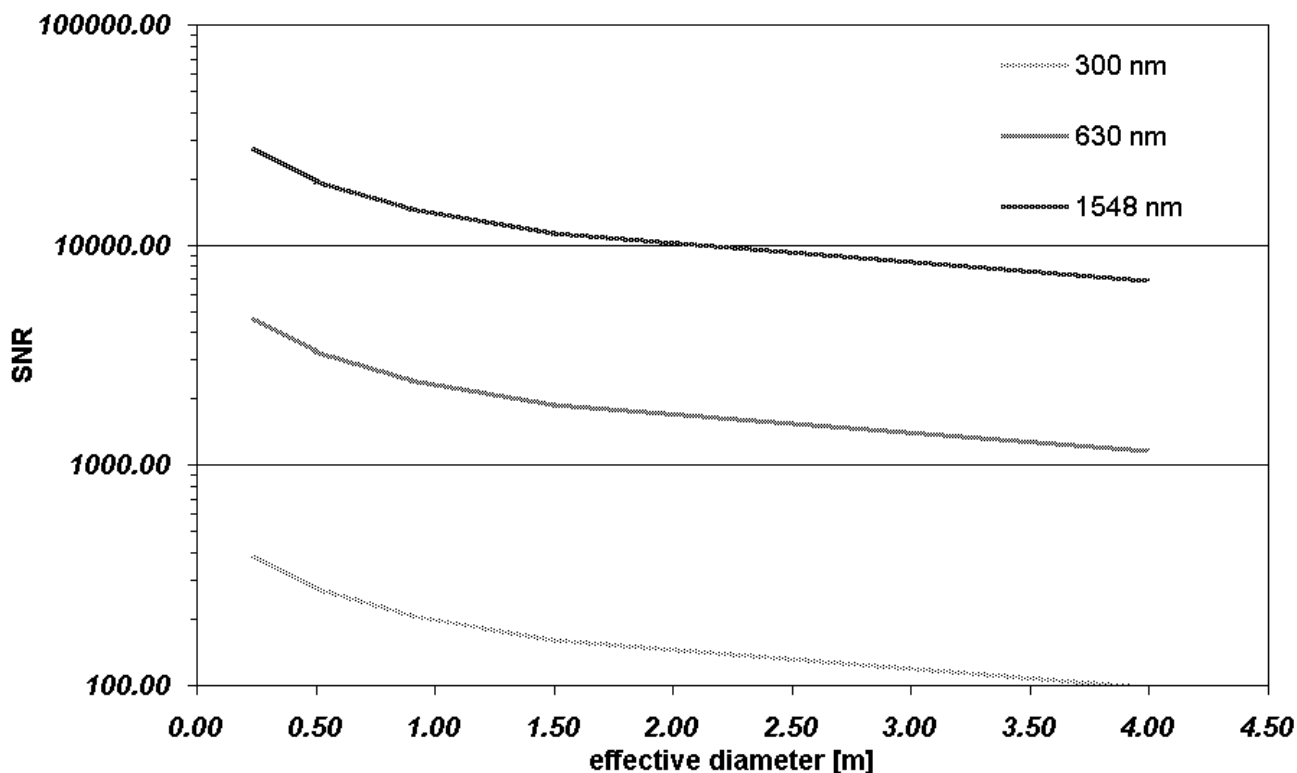


Fig. 2: Maximum signal-to-noise ratio (SNR) at the diffraction limit as a function of telescope aperture. The maximum SNR is determined by the number of photons that can be collected during the maximum exposure time given in Fig. 1.

Figures 1 and 2 show the maximum exposure time and the maximum possible SNR as a function of telescope diameter for three different wavelengths. For a 4-m aperture telescope such as the ATST and in the visible, a maximum exposure time of about 1 second is possible, which leads to a maximum SNR of about 1000. For polarimetry, the maximum possible SNR needs to be reduced by about a factor of 2 because of the added complexity involved in measuring polarization. Typical polarimetric signal levels from solar features are only a few percent, and many interesting magnetic field diagnostics require high SNR measurements of these small polarization signals. It is therefore challenging to carry out polarimetry close to the diffraction limit of a solar telescope, and it gets more and more challenging with increasing aperture.

3. SPECKLE IMAGING

Polarimetric observations with spatial pixel sizes appropriate for diffraction-limited resolution and spectral pixel sizes adequate to resolve polarized spectral line profiles require exposure times of at least 1 second to achieve a useful SNR. Atmospheric seeing therefore always degrades the spatial resolution of ground-based, polarimetric solar observations. Hence a variety of techniques have been developed to minimize the degrading influence of seeing. As already mentioned in the introduction, current solar adaptive optics systems do not fully compensate atmospheric aberrations. To reach the ultimate spatial resolution, it is therefore still necessary to use post-facto reconstruction techniques even when using adaptive optics. The reconstruction techniques typically operate on images and not on spectrograms. Therefore, high spatial resolution polarimetric observations have typically been obtained with narrow-band tunable filters.

Speckle imaging relies on a number of short exposure measurements (about 10 ms exposure time in the visible part of the spectrum) that are combined in such a way as to preserve the diffraction limited information that is present in the individual exposures, but which is absent in the arithmetically averaged data corresponding to a long-exposure measurement. Speckle imaging assumes that the structure of the observed object does not change during the collection of the short-exposure images. Detailed reviews of solar speckle imaging can be found elsewhere^{5,6}.

To understand some of the issues faced when reconstructing polarimetric solar images, it is helpful to briefly review speckle imaging as applied to solar observations. Image formation through the turbulent atmosphere of the Earth can be described by the incoherent, space-invariant imaging equation. The observed images I in the Fourier domain are given by

$$I = OS.$$

O describes the Sun outside of the Earth's atmosphere and is assumed to be time-independent. S is the optical transfer function (OTF), which varies with time since it includes the influence of seeing. Aberrations due to the atmosphere strongly depend on the location of a given source at one moment in time because the telescope beam corresponding to different sources traverses different parts of the atmosphere. However, if we select a small enough angular extent, the isoplanatic patch, we may assume that the aberrations are the same for all points in this patch. Therefore, the formulation above is only correct within an angular area of the size of the isoplanatic patch, which is typically a few seconds of arc for day-time seeing conditions.

The reconstruction of O is typically performed separately for its amplitudes and phases. The amplitudes of O_b are reconstructed with the Labeyrie⁷ technique by calculating the average power spectrum of the image series. Applying the same technique to a narrow-band channel is possible in principle, but the much-reduced SNR in narrow spectral bands renders this unpractical. The average power spectrum is the product of the OTF modulus squared and the so-called speckle transfer function (STF). Since the power spectrum of a point source is constant with spatial frequency, the average power spectrum of a point source is the STF. In the absence of a point source on the Sun, the STF is determined from model calculations of the Earth's atmosphere. The phases of O can be restored with a variety of techniques⁸⁻¹². After combination of the separately reconstructed amplitudes and phases of the Fourier transform of the object, the true object is obtained via inverse Fourier transformation. The reconstructions are performed in small, overlapping segments to account for anisoplanatism. After the restoration process the segments are recombined to cover the full field of view.

The major problem in speckle imaging of solar features is the absence of point sources to calibrate the Fourier amplitudes of the object. Although models of the atmospheric turbulence have been used with good success, it might not always be a sufficiently good approximation of reality. It is even more difficult to model the STF for images taken behind an adaptive optics system. While such corrections have been made¹³, they have to make many simplifying assumptions about the actual AO system. Hence the amplitudes of the speckle reconstruction are limited in accuracy by the restricted reliability of the model of the turbulent atmosphere and, if applicable, of the performance of the AO system. Yet another problem is due to telescope aberrations. Their influence is not taken into account when calibrating the Fourier amplitudes of the object, and the phase reconstruction is also affected. Fortunately, the influence of telescope aberrations on the restoration is not significant as long as they are much smaller than the distortions induced by the atmosphere, which is often the case.

4. PHASE DIVERSE SPECKLE IMAGING

A wavefront sensor that directly measures the combined wavefront aberrations due to the atmosphere, the telescope, and the instrument circumvents both the model-dependent amplitude calibration and the influence of unknown fixed telescope and instrument aberrations. In principle, one could use a Shack-Hartmann wavefront sensor as is used for solar adaptive optics. An example of such a reconstruction is shown in Fig. 4. However, like adaptive optics, such an approach also suffers from anisoplanatism, i.e. it only works over a very limited field of view.

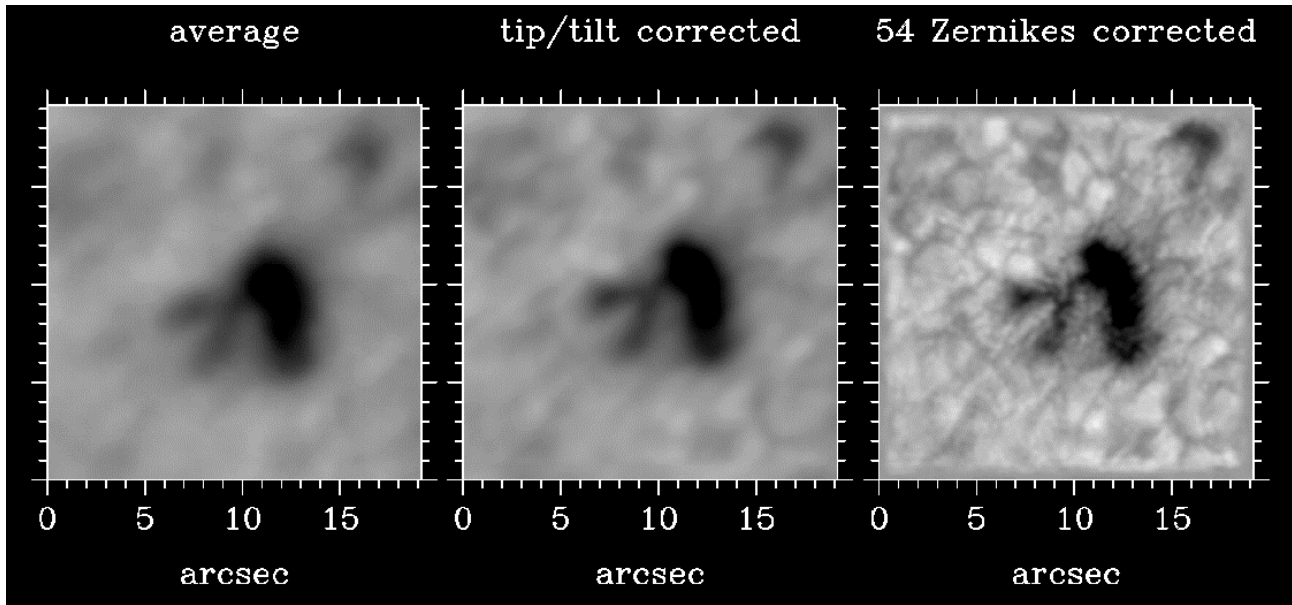


Fig. 3: The three pictures were derived from 100 simultaneous short-exposure images of a small sunspot at 1000 nm and the corresponding wavefront sensor data obtained with the 1.5-m McMath-Pierce solar telescope. The left image corresponds to the average of all 100 images, the center image represents the average after correcting for image motion (which simulates the effect of a correlation tracker), and the right image shows the deconvolved image using the first 54 Zernike components of the measured wavefront aberrations.

A much better suited type of wavefront sensor is provided by phase diversity, which, in its simplest form, uses a focused image and a deliberately, simultaneously collected, defocused image. Object and wavefront estimates can be obtained from a single image pair¹⁴ or from a series of pairs for a more reliable estimate^{15,16}. The latter is also called phase-diverse speckle imaging because it uses a series of pairs. A detailed description of phase diversity and a comparison of the two most common implementations with speckle imaging has been prepared by Paxman et al.¹⁷.

As is done with speckle imaging, phase diversity also reconstructs images in small, overlapping segments the size of an isoplanatic patch that are combined to deliver diffraction-limited images over a large field of view. Since phase-diversity also provides estimates of the instantaneous wavefront aberration as a function of field position, it is very useful in assessing the performance of an AO system.

5. SPECKLE DECONVOLUTION

Attempts to use conventional speckle imaging with narrow-band spectro-polarimetric observations have failed¹⁸. As seen in Section 2, a narrow spectral band contains a limited number of photons. While thousands of images may be collected over periods of hours to achieve a useful SNR in nighttime applications, this is not applicable to observations of rapidly changing solar structures. Furthermore, most nighttime applications of speckle imaging involve the restoration of a set of point sources whose power spectrum is independent of the spatial frequency (when neglecting diffraction at the telescope aperture). In contrast, the power spectrum of typical solar structures shows an exponential decrease with increasing spatial frequency. Therefore, solar speckle imaging needs a SNR in the short-exposure images that is orders of magnitudes higher than for typical nighttime applications, and this is why spectro-polarimetric images are almost impossible to reconstruct directly.

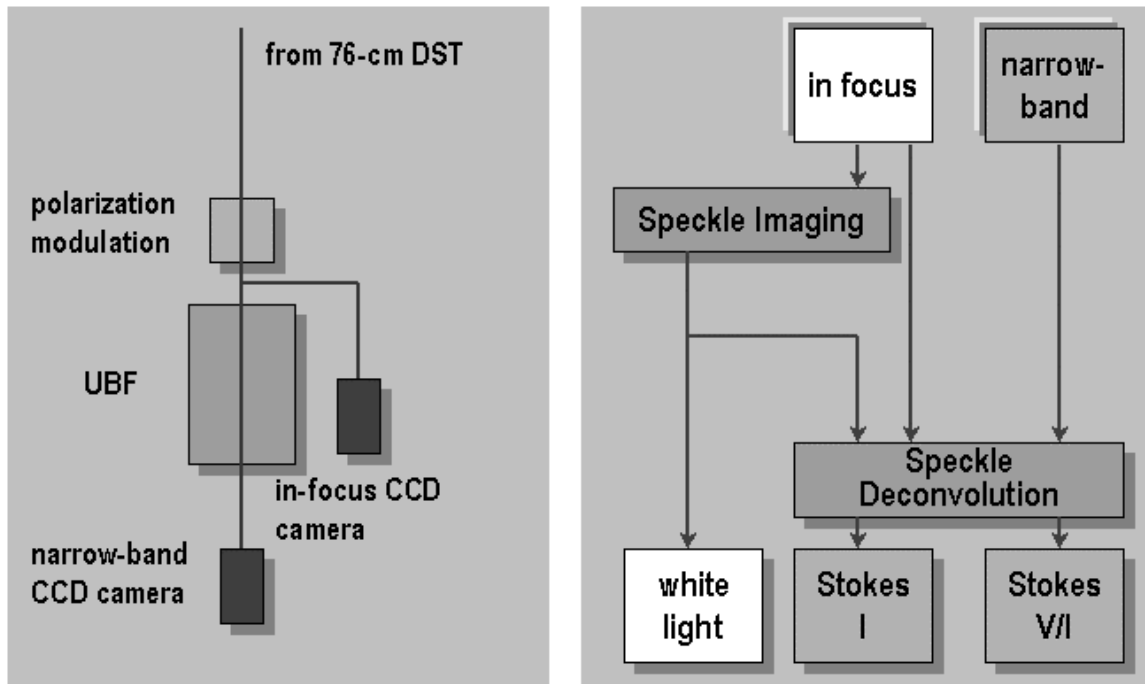


Fig. 4: Schematic diagrams showing the optical setup (left) and the data reduction flow (right) for speckle imaging, speckle deconvolution, and speckle polarimetry as used at the Dunn Solar Telescope of the National Solar Observatory in Sunspot, New Mexico.

A method to overcome the resolution limit of narrow-band filter images was developed by Keller and von der Lühe¹⁹. This *speckle deconvolution* technique provides near-diffraction-limited filtergrams by combining short-exposure images from a narrow-band and a broad-band channel. When speckle deconvolution is applied to polarization measurements in the wings of a Zeeman sensitive line, the technique is called *speckle polarimetry*. Various results have been reported²⁰⁻²².

The basic idea of speckle deconvolution consists in realizing that narrow spectral bands are not required for speckle imaging and that speckle imaging methods are not required for narrow-band imaging. The broad-band channel (about 10 nm wide) is used to determine the instantaneous point spread function (PSF). The simultaneous narrow-band images (about 0.01 nm wide) are deconvolved with this PSF. The image formation in the Fourier domain can again be written as

$$I_b = O_b S, \quad I_n = O_n S,$$

where the subscripts b and n denote the simultaneously observed broad and narrow-band channels, respectively. If the two pass-bands are sufficiently close, we may assume that both channels are subject to the same OTF. Conventional speckle imaging or phase-diverse speckle imaging is used to obtain an estimate of the true solar scene in the broad-band channel, O_b (in Fourier space). The best estimate for the narrow-band scene is the given by

$$O_n = O_b \frac{\langle I_n I_b^* \rangle}{\langle I_b I_b^* \rangle}.$$

Direct deconvolution is not possible because of discrete zeroes in the OTF, S . However, by taking a weighted ensemble average, indicated with brackets, the sum of noisy quotients can be replaced by a single, less noisy quotient. It is easy to show that the approximation as calculated with the weighted average is indeed identical to the true object in the narrow-band channel. A detailed description of speckle deconvolution and further discussions of the influence of noise may be found in Keller and von der Lühe¹⁹.

The SNR of the reconstructed narrow-band channel is approximately given by the geometric mean of the SNR in the two channels²³. This explains the major improvement of speckle deconvolution over direct speckle imaging in the narrow-band channel. The SNR in the broad-band channel may easily be a factor of 100 larger than in the narrow-band channel.

Then the speckle deconvolution reconstruction has a factor of 10 better SNR than the direct speckle imaging approach. Figure 5 shows an example of data sets obtain with this approach. The sampling pixel size of those observations does not allow us to reach the diffraction limit of the telescope, but it is an optimum size to achieve the high signal-to-noise ratio required for speckle polarimetric observations of network magnetic fields. Keller and Wilton²² show more results.

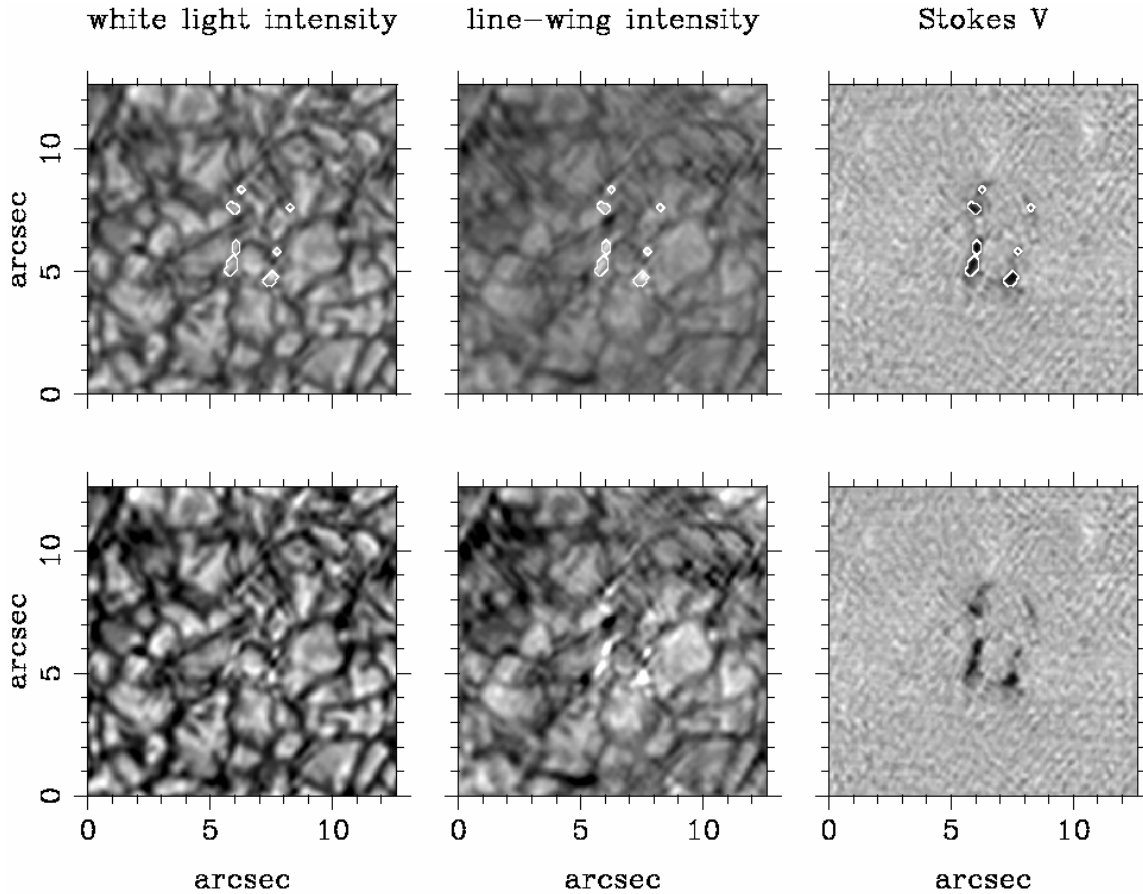


Fig. 5: An example of a high-resolution observation of network magnetic fields close to disk center using speckle polarimetry. The lower three images are the same as the upper two except for a different gray-scale and the absence of contour lines that indicate the location of concentrated magnetic fields.

6. COMBINED ADAPTIVE OPTICS AND PHASE DIVERSE SPECKLE IMAGING

As mentioned above, phase-diverse speckle imaging is particularly well suited to be combined with adaptive optics. Together with Rick Paxman, John Seldin, Dave Carrara, and Thomas Rimmele, I have combined the low-order adaptive optics system at the Dunn Solar Telescope with a versatile polarimeter (ZIMPOL I, see below) and used phase-diverse speckle imaging and speckle deconvolution to obtain diffraction-limited time sequences of magnetic fields²⁴. The adaptive optics²⁵ was correcting the low-order aberrations (24 subapertures over the 76-cm telescope aperture) with an update rate of about 1.5 kHz. A narrow-band channel with the Universal Birefringent Filter in the wing of the CaI 610.3 nm line and two white-light channels were used to obtain simultaneous in-focus and out-of-focus images for the phase-diversity processing as well as circular polarization measurements in the narrow-band channel. All three channels were equipped with a ZIMPOL I camera running simultaneously at 5 frames per second. Figure 6 provides an overview of the optics as well as the data processing approach.

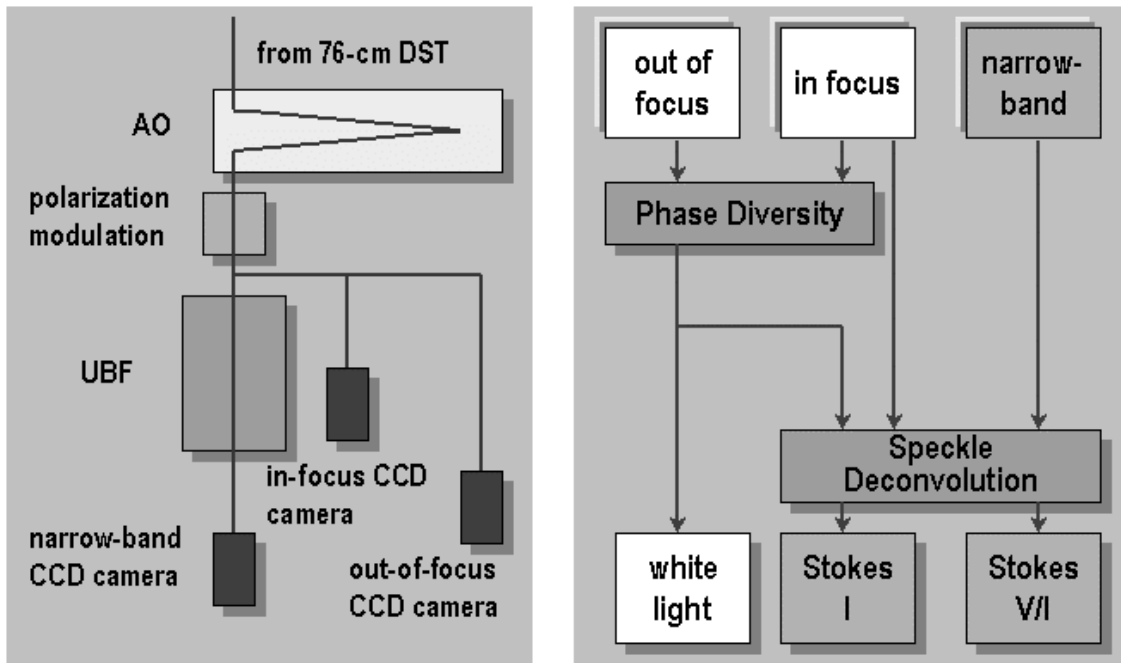


Fig. 6: Schematic diagrams showing the optical setup (left) and the data reduction flow (right) for combined adaptive optics and phase-diverse speckle polarimetry.

Out of every 100 image triplets, the 20 sharpest white-light in and out-of-focus images were selected to determine the true solar image and the corresponding wavefront aberrations. Then we used 100 in-focus white light images and the phase-diverse speckle reconstruction to determine 100 spatially varying point spread functions, with which the simultaneous Stokes I and V images were deconvolved. The reconstructed white-light, narrow-band line wing, and magnetogram time sequences were destretched to remove spatially varying image motion. Finally, a subsonic filter was applied to limit apparent pattern speeds to less than 5 km/s, which reduces the noise considerably without removing any true solar feature. Figure 7 shows a single time step out of this 19-minute time series.

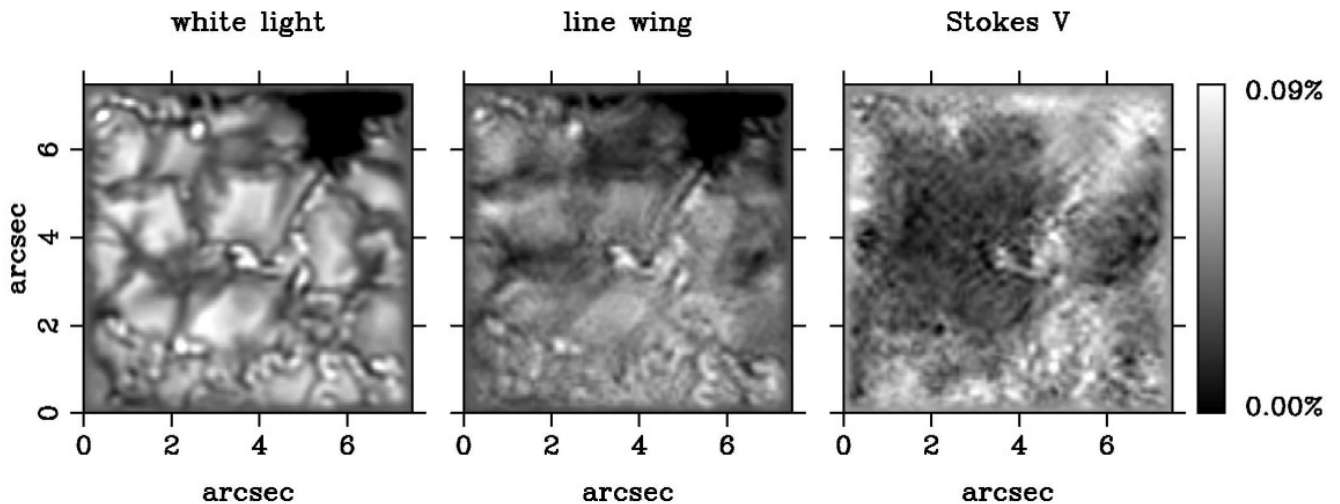


Fig. 7: The distance between the two clearly separated magnetic elements in the center of the field of view is only 0.3 arcsec showing the excellent spatial resolution (the diffraction-limit of the telescope at 610 nm is 0.16 arcsec). The gray-scale bar on the far right indicates the scaling used for Stokes V, which was normalized with the average line wing intensity. Since all magnetic fields in this area had the same polarity, there is no negative flux, and therefore black corresponds to no magnetic flux.

7. INSTRUMENTAL DEVELOPMENTS

It is clear from Section 2 that diffraction-limited polarimetry at large-aperture solar telescopes must pay careful attention to several issues. Optics and detectors must be highly efficient, i.e. light losses in polarization modulators must be minimized; multilayer coatings on optical elements are required; and high-speed array detectors with quantum efficiencies close to unity are urgently needed. High-speed array detectors are needed to make use of all the photons that hit the detector within the maximum possible integration time (a few seconds at most, see Section 2). Since array detectors have rather limited full-well capacities (typically a few 100,000 electrons per exposure), an array detector needs to be read out often and quickly. A realistic goal is to achieve an overall efficiency of the combined telescope and instrument of 30%. Furthermore, there is no time for scanning in space or wavelength, which makes the use of integral field units such as fiber fed spectrographs, image slicers, lenslet arrays etc. a necessity. Nevertheless, most polarimetry will not be carried out at the diffraction limit, at least in the visible part of the spectrum, because of the photon starvation at the diffraction limit (see Section 2).

The most crucial ingredient in any future polarimeter that operates close to the diffraction limit of a large solar telescope is a high-speed, high-sensitivity array detector that is suitable for polarimetry. The Zurich Imaging POLarimeter (ZIMPOL) I and II represent the first detector concepts that were specifically designed for solar polarimetry. The polarization modulation is best done at frequencies much faster than the seeing and the update rate of AO systems, i.e. above 1 kHz. However, this is incompatible with the read-out rate of large, sensitive array detectors. A new instrument concept developed by Povel et al²⁶ reconciled the incompatibility by using a CCD directly as a part of the demodulator. The array is alternately divided into photosensitive rows and storage rows that are shielded from light by an opaque mask. The photo charges generated in the photosensitive rows during the first modulation half-cycle are shifted into the adjacent storage row at the transition to the second modulation half-cycle. The photo charges generated during the second modulation half-cycle are shifted into the opposite, adjacent storage row at the transition to the first modulation half-cycle. This procedure is repeated over many modulation cycles until the desired amount of charges have been accumulated. Then the CCD array is read out. Pixel-to-pixel gain variations do not affect the measured fractional polarization. To avoid a reduction of the measured modulation amplitude due to the finite transfer time, charges must be shifted about a factor of 100 faster than the modulation frequency. Furthermore, the charge transfer efficiency in both directions needs to be very high.

ZIMPOL I is based on 42-kHz polarization modulation with piezo-elastic modulators and custom 393 by 284 pixel CCD sensors²⁷. It can operate up to four cameras simultaneously at a rate of up to 10 frames per second. This enables precise polarization measurements even with the short exposure times required for speckle imaging. Drawbacks include the low efficiency due to the mask (a factor of 2) and the restriction of a single CCD demodulator to one frequency (a factor of 3 for vector-polarimetry). This total efficiency loss of a factor of 6 is overcome by ZIMPOL II^{28,29}. Four sampling intervals in one modulation cycle are needed to record all four modulation states. The light is focused on the CCD with a micro-lens array such that out of four pixels in one column only one is used for light detection while the remaining three are used for temporary charge storage. In this way all four Stokes parameters may be measured with a single CCD sensor. While possible, it proved hard to accurately align the micro-lenses on the CCD³⁰. Furthermore, stray-light within the micro-lens-CCD assembly led to significant problems during the data reduction. Finally, it has not been possible to adapt the scheme to a backside-illuminated CCD that would have provided the desired high quantum efficiency nor to adapt it to infrared detectors.

New developments in hybrid detector arrays have opened the possibility to build the perfect array detector for polarimetry as envisioned by Lites³¹. The HyViSI hybrid CMOS silicon arrays by Rockwell Scientific provide the advantages of a backside-illuminated CCD with the flexibility, speed, and cost-efficiency of a CMOS imager. The HyViSI arrays are based on the same CMOS hybrid technology as the well-known Rockwell infrared arrays. Silicon is used instead of HgCdTe, which makes the arrays sensitive to visible and ultraviolet light. The same read-out multiplexer can be used for either infrared or HyViSI arrays. 1024 by 1024 pixel HyViSi cameras are available as a commercial product. 2048 by 2048 arrays are in the engineering phase.

A typical CMOS multiplexer contains two capacities, one of which is used for integrating the charges of the current exposure, while the other holds the charges from the previous exposure that is concurrently read out. Instead of only 2

capacities, one could imagine 8 capacities within every pixel. Figure 8 shows an outline of one pixel of such a device. Since an 18- μm pixel can hold about 6,000,000 electrons, a full-well depth of more than 500,000 would still be possible for every 18- μm pixel and every polarization modulation state. Larger pixel sizes would offer even larger full-well depths. The charges from the silicon would then be sent to one of four capacities in synchrony with the polarization modulation. Before the next image is exposed, the four integrating capacities would transfer their charges to the four read-out capacities. The cost for the design of such a new CMOS multiplexer is on the order of \$500,000. Such a multiplexer could then be hybridized with either silicon to cover the 300 nm to 1100 nm wavelength range, or with HgCdTe to cover the 1000 nm to 5000 nm infrared wavelength range.

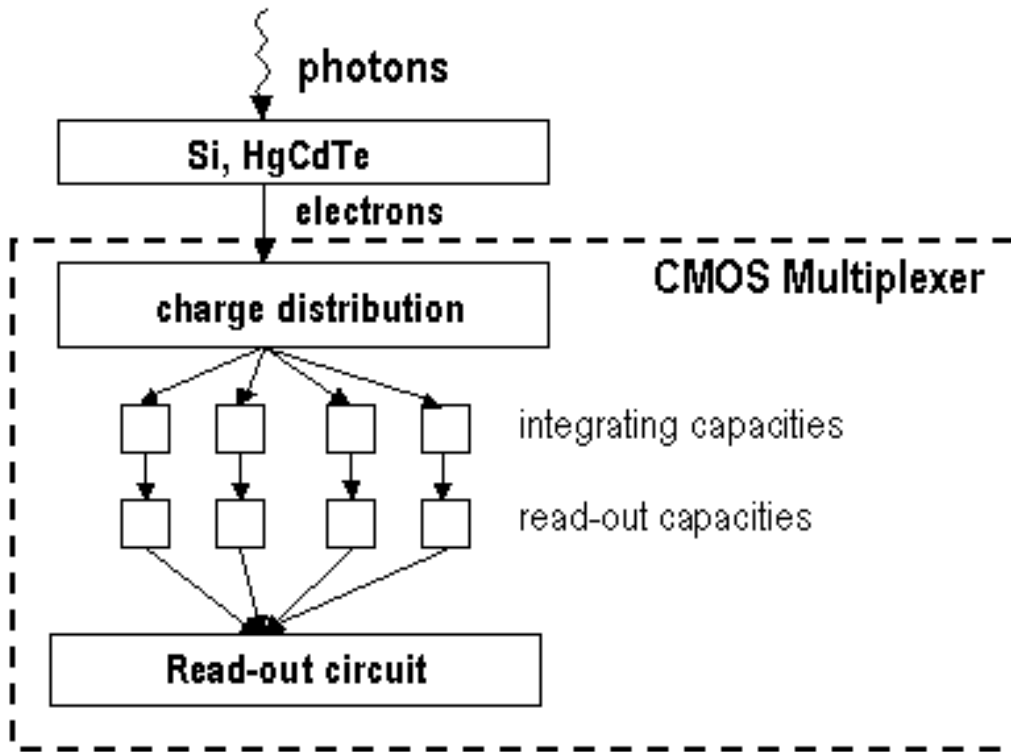


Fig. 8: Schematic layout of a single pixel of a new CMOS hybrid array detector that is capable of measuring all four Stokes parameters. It has a 100% geometric fill factor and very high quantum efficiency. The photosensitive layer can be chosen such as to cover the 300-1100 nm or the 1000-5000 nm wavelength ranges.

8. CONCLUSIONS

The combination of adaptive optics and post-facto image reconstruction provides the basic tool to obtain diffraction-limited polarimetric time sequences over a substantial field of view with current and future solar telescopes. Until the advent of reliable MCAO, this will remain the technique of choice for polarimetry close to the diffraction limit over a substantial field of view. Still, improvements in telescopes, instruments, and image reconstruction techniques are needed to make further progress. Since the diffraction limit of current solar telescopes can be reached, it is crucial to build larger solar telescopes such as the 4-m ATST². Such telescopes should be as free of instrumental polarization as possible. Future instruments need to have higher throughput and efficiency than current instruments, and polarimeters need to measure the polarization accurately even within the short exposure times required for post-facto image reconstruction. New detector concepts such as the one introduced in the previous section might be crucial to achieve this.

Image reconstruction techniques need to be improved too. In particular, an open-source version of the highly successful phase-diverse speckle code developed by Paxman and colleagues¹⁵⁻¹⁶ is needed. Furthermore, the reconstruction

approaches must be extended to long-slit spectrograph observations. While a general approach has been successfully worked out³², it has so far only been applied to intensity measurements.

ACKNOWLEDGEMENTS

Dave Carrara, Kurt Gleichman, Rick Paxman, John Seldin, Thomas Rimmele, and Bruce Wilton all made significant contributions to the observations shown here. The National Solar Observatory is operated by the Association of Universities for Research in Astronomy, Inc. (AURA) under cooperative agreement with the National Science Foundation.

REFERENCES

1. R.F. Stein, Å. Nordlund, "Realistic solar convection simulations", *Solar Physics* **192**, pp. 91–108, 2000.
2. S.L. Keil, T. Rimmele, C.U. Keller, "Design and Development of the Advanced Technology Solar Telescope", *SPIE* **4853**, submitted, 2002.
3. T.R. Rimmele, "Solar adaptive optics", *SPIE* **4007**, pp. 218-231, 2000.
4. G.B. Scharmer, M. Shand, M.G. Lofdahl, P.M. Dettori, W. Wei, "Workstation-based solar/stellar adaptive optics system", *SPIE* **4007**, pp. 239-250, 2000.
5. C. Aime, in Proceedings of the 10th Sacramento Peak Summer Workshop, Sunspot, New Mexico, pp. 127, 1989.
6. O. von der Lühe, "High spatial resolution solar observations", Proceedings of the 10th Sacramento Peak Summer Workshop, Sunspot, New Mexico, pp. 147, 1989.
7. A. Labeyrie, "Attainment of Diffraction Limited Resolution in Large Telescopes by Fourier Analysing Speckle Patterns in Star Images", *A&A* **6**, pp. 85-87, 1970.
8. K.T. Knox, B.J. Thompson, "Recovery of images from atmospherically degraded short-exposure photographs", *ApJ* **193**, L45-L48, 1974.
9. O. von der Lühe, "Speckle imaging of solar small scale structure. I – Methods", *A&A* **268**, 374-390, 1993.
10. A.W. Lohmann, G. Weigelt, B. Wirtzner, "Speckle masking in astronomy - Triple correlation theory and applications", *Appl. Optics* **22**, pp. 4028-4037, 1983.
11. E. Pehlemann, O. von der Lühe, "Technical aspects of the speckle masking phase reconstruction algorithm", *A&A* **216**, 337-346, 1989.
12. C.R. de Boer, F. Kneer, "Speckle observations of abnormal solar granulation", *A&A* **264**, pp. L24-L26, 1992.
13. O. von der Lühe, private communication, 2001.
14. M.G. Lofdahl, G.B. Scharmer, "Wavefront sensing and image restoration from focused and defocused solar images", *A&ASS* **107**, pp. 243-264, 1994.
15. R.G. Paxman, J.H. Seldin, "Fine-resolution astronomical imaging with phase-diverse speckle", *SPIE* **2029**, pp. 287-298, 1993.
16. J.H. Seldin, R.G. Paxman, "Phase-diverse speckle reconstruction of solar data", *SPIE* **2302**, pp. 268-280, 1994.
17. R.G. Paxman, J.H. Seldin, M.G. Lofdahl, G.B. Scharmer, C.U. Keller, "Evaluation of Phase-Diversity Techniques for Solar-Image Restoration", *ApJ* **466**, pp. 1087-1099, 1996.
18. J.W. Harvey, in Small Scale Magnetic Flux Concentrations in the Solar Photosphere. Vandenhoeck and Ruprecht, Göttingen, pp. 25, 1986.
19. C.U. Keller, O. von der Lühe, "Solar speckle polarimetry", *A&A* **261**, pp. 321-328, 1992.
20. C.U. Keller, "Resolution of magnetic flux tubes on the sun", *Nature* **359**, pp. 307-308, 1992.
21. C.U. Keller, "Properties of solar magnetic fields from speckle polarimetry", *Reviews in Modern Astronomy* **8**, pp. 27–59, 1995.
22. C.U. Keller, B.P. Wilton, "Properties of Solar Network Magnetic Elements from Speckle Polarimetry", *ApJ*, in preparation.
23. R. Petrov, F. Roddier, C. Aime, "Signal-to-noise ratio in differential speckle interferometry", *JOSA* **A3**, pp. 634-644, 1986.
24. J.H. Seldin, R.G. Paxman, D.A. Carrara, C.U. Keller, T.R. Rimmele, "Deconvolution of Narrow-Band Solar Images Using Aberrations Estimated from Phase-Diverse Imagery", *SPIE* **3815**, pp. 155-163, 1999.
25. T.R. Rimmele, "Solar adaptive optics", *SPIE* **4007**, pp. 218-231, 2000.

26. H.P. Povel, H. Aebersold, J.O. Stenflo, "Charge Coupled Device Image Sensor as a Demodulator in a 2D Polarimeter with piezo-elastic Modulators", *Appl. Optics* **29**, pp. 1186-1190, 1990.
27. H.P. Povel, "Imaging Stokes polarimetry with piezoelastic modulators and charge-coupled-device image sensors", *Opt. Eng.* **34**, pp. 1870-1878, 1995.
28. J.O. Stenflo, C.U. Keller, H.P. Povel, "Demodulation of all Four Stokes Parameters With a Single CCD. ZIMPOL II Conceptual Design", *LEST Technical Report* **54**. University of Oslo, 1992.
29. A.M. Gandorfer, H.P. Povel, "First observations with a new imaging polarimeter", *A&A* **328**, pp.381-389, 1997.
30. M.T. Gale, J. Pedersen, H. Schuetz, H. Povel, A. Gandorfer, P. Steiner, P. Bernasconi, "Active alignment of replicated microlens arrays on a charge-coupled device imager", *Opt. Eng.* **36**, pp. 1510-1517, 1997.
31. B.W. Lites, Proceedings of the Eleventh Sacramento Peak Summer Workshop, New Mexico, 1991.
32. C.U. Keller, A. Johannesson, "Speckle spectrography of extended objects", *A&ASS* **110**, pp. 565-571, 1995.